The effect of pH and ionic strength on proton adsorption by the thermophilic bacterium *Anoxybacillus flavithermus*

Peta-Gaye Burnett [a,*], Hannah Heinrich [b], Derek Peak [a], Phil J. Bremer [c],
A. James McQuillan [b], Christopher J. Daughney [d]

[a] *Department of Soil Science, University of Saskatchewan, 51 Campus Drive, Saskatoon, SK, Canada S7N 5A8*
[b] *Department of Chemistry, University of Otago, Dunedin, New Zealand*
[c] *Department of Food Science, University of Otago, Dunedin, New Zealand*
[d] *Institute of Geological and Nuclear Sciences, Lower Hutt, New Zealand*

Abstract

Numerous studies have utilized surface complexation theory to model proton adsorption behaviour onto mesophilic bacteria. However, few experiments, to date, have investigated the effects of pH and ionic strength on proton interactions with thermophilic bacteria. In this study, we characterize proton adsorption by the thermophile *Anoxybacillus flavithermus* by performing acid–base titrations and electrophoretic mobility measurements in $NaNO_3$ (0.001–0.1 M). Equilibrium thermodynamics (Donnan model) were applied to describe the specific chemical reactions that occur at the water–bacteria interface. Acid–base titrations were used to determine deprotonation constants and site concentrations for the important cell wall functional groups, while electrophoretic mobility data were used to further constrain the model. We observe that with increasing pH and ionic strength, the buffering capacity increases and the electrophoretic mobility decreases. We develop a single surface complexation model to describe proton interactions with the cells, both as a function of pH and ionic strength. Based on the model, the acid–base properties of the cell wall of *A. flavithermus* can best be characterized by invoking three distinct types of cell wall functional groups, with pK_a values of 4.94, 6.85, and 7.85, and site concentrations of 5.33, 1.79, and 1.42×10^{-4} moles per gram of dry bacteria, respectively. *A. flavithermus* imparts less buffering capacity than pure mesophilic bacteria studied to date because the thermophile possesses a lower total site density (8.54×10^{-4} moles per dry gram bacteria).
© 2006 Elsevier Inc. All rights reserved.

1. Introduction

Bacterial cell walls possess proton-active functional groups that are ionized as a function of environmental pH (e.g. Beveridge and Murray, 1980; Beveridge et al., 1982; Beveridge, 1989; Fein et al., 1997; Daughney et al., 1998; Wightman et al., 2001; Yee and Fein, 2001; Borrok et al., 2004a,b). Deprotonation of these functional groups confers electrostatic charge to the cell periphery and gives the cell wall anionic characteristics and metal binding ability. Adsorption of metals by bacteria can influence the distribution and transport of metals in natural and engineered

water–rock systems. The ubiquity of bacteria in natural systems, coupled with the fact that they are efficient metal sorbents (high surface area to volume ratio provides a large contact area for bacteria–metal interactions), makes biosorption an active area of study.

Although many researchers have studied the adsorption of ions onto bacteria, few investigations have been conducted with thermophilic bacteria. Moderate thermophiles grow most efficiently at temperatures ranging from approximately 45–80 °C (Brock, 1986; Madigan, 2000; Chapelle, 2001; Sampson and Phillips, 2001) and are typically associated with continental geothermal regions and submarine hydrothermal vents. Wightman et al. (2001) investigated proton adsorption by a thermophilic isolate grown at 50 °C. These authors reported that the bacterial surface site

---

* Corresponding author. Fax: +1 30 69 666 881.
  E-mail address: pete.burnett@usask.ca (P.-G. Burnett).

deprotonation reactions were not strongly temperature dependent, and concluded that both the thermophilic isolate and the mesophile *Bacillus subtilis* displayed three different types of proton-active cell wall functional groups with comparable pK_a values (4.5, 5.8, 8.2 for the thermophile and 4.1, 5.8, 7.7 for *B. subtilis*). These authors assumed that, like other bacteria, the thermophile possessed net negative electrostatic surface charge at neutral pH. However, based on the single study by Wightman et al. (2001), it is not yet clear whether or not ion adsorption by other thermophiles will parallel that of bacteria grown at lower temperatures.

In this study, we examine the effects of pH and ionic strength on the acid–base properties and charging behaviour of the thermophile *Anoxybacillus flavithermus* in late stationary phase. We assess cell wall charge density by performing acid–base titrations and electrophoretic mobility measurements. We describe the experimental data by using surface complexation models (SCMs) to quantify surface site concentrations and proton-binding stability constants. We employ a Donnan electrostatic model, in which binding sites are distributed throughout a volume, not just located at the plane at the cell-solution interface (see also Plette et al. (1995), Martinez et al. (2002) and Yee et al. (2004)). Our objectives are: (1) to develop a SCM to characterize proton adsorption by the thermophile; (2) to investigate whether or not the SCM parameters (deprotonation constants and site concentrations) can be used to predict electrophoretic mobility; and (3) to compare proton sorption by the thermophile to a range of other bacteria based on data from the literature.

2. Methods

2.1. Preparation of bacterial suspensions

Anoxybacillus flavithermus was isolated from the main wastewater drain at the Wairakei Geothermal Power Station (Wairakei, North Island, New Zealand) as described by Mountain et al. (2003). The wastewater is ~60 °C, pH 8.2, with Na^+ and Cl^- as the major ions (1127 and 1858 ppm, respectively) and 559 ppm SiO_2. Water samples were aseptically collected from the drain, used to inoculate liquid growth media, and then incubated at 60 °C. Pure cultures were obtained by sub-culturing on solid media to obtain colonies of a single morphotype. Pure cultures were subsequently identified by PCR amplification of 16 S rDNA followed by analysis with an ABI 337 automated sequencer (Perkin Elmer, Applied Biosystems). The isolate used in our experiments had >97% homology with *A. flavithermus*, based on the Basic Local Alignment Search Tool (BLAST) network service (Altschul et al., 1990).

The bacteria were precultured in 5-mL volumes of autoclaved (121 °C for 20 min) trypticase soy broth (Becton, Dickinson and Company, USA). After growing for 24 ± 0.1 h at 60 °C, either two or three of the 5-mL precultures were transferred to a 1-L volume of autoclaved broth, which was then placed in an orbital mixer incubator (100 rpm) at 60 °C. Growth curves were obtained by constructing graphs of optical density at 600 nm (OD_{600}) over time. The 1-L culture was harvested after 24 ± 0.1 h when the cells were in late stationary phase. Bacterial cells were removed from the growth medium by centrifugation ($2510g$, 20 min or $8230g$, 15 min) and rinsed three times in 0.01 M $NaNO_3$. After each step in the wash procedure, the bacteria were pelleted by centrifugation ($2510g$, 20 min or $8230g$, 15 min) and the supernatant was discarded. Within 15 min of the final rinse, the bacterial pellet was resuspended in a known weight of 0.01 M $NaNO_3$ (30–150 g, depending on the experiment to be performed). The suspension was then homogenized by vigorous shaking (15 min). This growth and rinsing protocol was followed to strip the cell walls of metals that may have been present in the growth medium, to leave the cells intact but metabolically inactive (Cox et al., 1999; Fein and Delea, 1999), and to remove any exudates that may have been present in the growth medium. The growth and rinsing protocol was also employed to ensure that our results would be comparable to previous investigations.

Biomass of the parent suspension was determined from OD_{600} relative to the electrolyte. The relationship between the OD_{600} of a bacterial suspension and the dry biomass was determined as follows: A known mass of suspension with known OD_{600} was filtered through a pre-weighed 0.45 μm filter membrane (Millipore) and flushed with distilled water several times. The filter was then placed in an oven and dried at 60 °C to constant weight. The increase in mass of the membrane was assumed to be equivalent to the dry mass of the bacteria. This procedure was repeated using cells from eleven independently grown cultures ($0.12 \leqslant OD_{600} \leqslant 1.50$), allowing a robust correlation between OD_{600} and biomass concentration (dry weight per litre) to be established. Similar protocols relating dry bacterial biomass to turbidity measurements have been employed in previous investigations (e.g. Banerjee et al., 1993).

The ratio of cell wet weight to cell dry weight was determined by a method commonly used (Fein and Delea, 1999; Daughney et al., 2001; Borrok et al., 2004a; Haas, 2004; Borrok and Fein, 2005). Weighed aliquots of the suspension were centrifuged at $5900g$ for 1 h. During this period, centrifugation was interrupted three times and the supernatant was discarded. After 1 h, the mass of the wet bacterial pellet was determined. The dry mass of the pellet was determined after oven drying at 60 °C to constant weight.

The bacterial cells were viewed under cryo-field emission scanning electron microscopy (cryo-FESEM) to determine cell dimensions. For cryo-FESEM, the bacteria were cut from a tryptic soy agar (TSA) plate, fixed in 2.5% glutaraldehyde (60 min), and post fixed in 1% osmium tetroxide (30 min). Samples were cooled to liquid nitrogen temperature (77 K) and coated with platinum. Samples were then viewed in a JEOL JSM-6700F field emission scanning electron microscope chamber (Tokyo, Japan) with an

accelerating voltage of 2.5 keV and 16,000× magnification. The cell dimensions were used to estimate surface area based on geometry (Fein et al., 1997; Wightman et al., 2001; Châtellier and Fortin, 2004; Daughney et al., 2004).

Cell wall thickness was measured on transmission electron microscopy (TEM) thin sections. For TEM, bacterial cells were scraped from a TSA plate and prepared using the ruthenium red method. Cells were primarily fixed in ruthenium red and 3% glutaraldehyde followed by a secondary fix in ruthenium red and 2% osmium tetroxide. The final washed and pelleted cells were combined with warm agarose (Sigma–Aldrich, USA). After solidification, 1 mm^3 sections of the sample were embedded in Quetol through stepwise dehydration with ethanol and infiltration of resin. These thin sections were viewed under a Philips CM 100 TEM (Eindhoven, Holland) at 100 kV. Three to five measurements per cell were taken. Cell wall thickness was used to estimate the cell wall volume (Wasserman and Felmy, 1998; Daughney et al., 2004).

Bacterial cells were examined before and after titrations using a BioRad MRC-1000 confocal scanning system (Hemel Hempstead, UK) equipped with a krypton–argon laser and mounted on a Nikon Microphot-SA microscope (Tokyo, Japan). Cells were fixed by flaming, then stained with either syto-9 and propydium iodide, or a lectin followed by syto-9, and viewed through a 60× oil immersion lens.

To investigate the possible release of exudates and metabolites from rinsed cell suspensions, dissolved organic carbon (DOC) concentrations in filtrates (0.45 μm) of bacterial suspensions collected after 2 h of equilibration at various pHs and ionic strengths were measured. These results were compared to control experiments, in which DOC was measured in filtrates immediately following the final rinse and resuspension in fresh electrolyte (pH 6, ionic strength 0.001, 0.01, or 0.1 M). All DOC analyses were performed using a Shimadzu TOC 5050A total organic carbon analyser (Kyoto, Japan) employing a non-purgeable organic carbon method.

2.2. Acid–base titrations

2.2.1. Ionic strength of 0.01 M

A known weight (50–120 g) of suspension containing cells from a single culture (0.38–0.74 dry g L^{-1}) was transferred into an air-tight polystyrene vessel. The pH was adjusted to ~4 by the addition of a known mass of standardized 0.144 M HNO$_3$, and the suspension was mixed with a magnetic stirrer and bubbled with humid CO$_2$-free N$_2$ gas for 30 min, to remove dissolved CO$_2$ from the suspension. The titration was conducted in an up-pH direction to pH 10 at 25 ± 1 °C using standardized CO$_2$-free 0.045 M NaOH and a Methrom titrator "736 GP Titrino" (Herisau, Switzerland) at the Wairakei Research Centre of the Institute of Geological and Nuclear Sciences (New Zealand). Throughout the duration of the titration, the suspension was continually stirred and bubbled with N$_2$ gas. Following each addition of titrant, the pH of the suspension

was recorded when a stability criterion of 5 mV/min was obtained. After the completion of most titrations, the suspension (ca. 120 g) was acidified to roughly pH 3.5, and a second up-pH titration was performed to investigate the reversibility of proton adsorption. The reproducibility of the experimental method was evaluated by performing duplicate titrations of two separate aliquots (ca. 50 g) of the parent suspension. The total volume of acid and base added, relative to the initial volume of the suspension, was such that the maximum dilution was ~10% (accounted for in modeling of the data). The entire procedure was conducted with five independently grown cultures, to examine inter-culture variability. These titrations are hereafter termed "0.01 M titrations." Control titrations of the electrolyte alone were performed on a regular basis to test for infiltration of CO$_2$ into the titrants and the experimental apparatus. A similar protocol has been followed by other researchers for titration of biological surfaces (Fein et al., 1997, 2005; Daughney et al., 1998, 2001, 2004; Yee and Fein, 2001; Claessens et al., 2004; Yee et al., 2004; Borrok et al., 2004a; Borrok and Fein, 2005).

2.2.2. Variable ionic strength of 0.001, 0.01, and 0.1 M

Prior to the final rinse step, the bacterial pellets from two independent cultures were combined to provide sufficient biomass for the subsequent experiments (0.21–0.27 dry g L^{-1}). Following the final rinse step, the bacterial pellet was resuspended in 0.01 M NaNO$_3$ (~30 g). The suspension was then divided among six reaction vessels (4 g each) to allow duplicate experiments to be conducted at ionic strengths of 0.001, 0.01, and 0.1 M. The 0.001, 0.01, and 0.1 M samples were prepared, respectively, as follows: by dilution with Milli Q water (36 g), by addition of 0.01 M NaNO$_3$ (36 g), and by addition of a known volume of 0.8 M NaNO$_3$ (4.95 g) and Milli Q water (31.05 g). Each suspension was then homogenized by vigorous shaking (15 min) and the OD$_{600}$, relative to the specific background electrolyte, was measured. The pH was adjusted to approximately 3.5 by the addition of a known aliquot of standardized 0.1 M HNO$_3$. Titrations were conducted in the up-pH direction at 22 ± 1 °C using a Methrom titrator "751 GP Titrino" (Herisau, Switzerland) and 730 sample changer at the University of Saskatchewan (Canada). The titrator was operated in an anaerobic chamber (Plas-Labs Inc., Michigan, USA) under a N$_2$ atmosphere. Standardized CO$_2$-free 0.01 M NaOH was used as the titrant. Following each addition of titrant, the pH of the suspension was recorded when a stability criterion of 6 mV/min was obtained. Due to difficulties encountered when attempting to titrate to pH 10 with bacterial suspensions of 0.001 M ionic strength, the upper pH limit of the titration range was reduced to ca. 9. The total volume of acid and base added, relative to the initial volume of the suspension, was such that the maximum dilution was ~10% (accounted for in modeling of the data). This procedure was conducted three times and these titrations are hereafter referred to as "ionic strength titrations." Control titrations of the

electrolyte alone were performed on a regular basis to test for infiltration of CO_2 into the titrants and the experimental apparatus.

2.3. Electrophoretic light scattering

For electrophoretic mobility measurements, bacterial cells were precultured in 2-mL volumes of autoclaved (121 °C for 20 min) trypticase soy broth (Becton, Dickinson and Company, USA). After growing for 24 ± 0.1 h at 57 °C, the preculture was transferred to a 200-mL volume of autoclaved broth, which was then placed in an oven set at 57 °C and constantly stirred. The 200-mL culture was harvested after 24 ± 0.1 h when the cells were in late stationary phase. Bacterial cells were removed from the growth medium by centrifugation (9820g, 8 min). The bacterial pellet was resuspended in 0.001 M $NaNO_3$ and evenly divided among three centrifuge bottles. Each suspension was made up to $\sim$150 g by the addition of 0.001, 0.01, and 0.1 M $NaNO_3$, respectively. The samples were centrifuged (9820g, 8 min) and the pellets rinsed twice in the respective electrolyte concentration. The final pellet was resuspended in the electrolyte (1 mL) and then stored on ice.

Aliquots (10 mL) of 0.001 M $NaNO_3$ were adjusted to different pH values (1.8–9.5) by addition of 1 M HNO_3 and 1 M NaOH, respectively. Immediately prior to electrophoretic mobility measurements, these samples were spiked with 0.001 M $NaNO_3$ bacterial suspensions (50–150 μL) and the final pH was measured. Electrophoretic mobilities were measured at 25 °C with a Malvern Zetasizer Nano ZS (Worcestershire, United Kingdom). Duplicate measurements were taken for all samples and averaged. Similar samples were prepared for 0.01 and 0.1 M ionic strengths. The electrophoretic mobilities of these samples were also measured. The entire procedure was conducted on three independently grown cultures.

2.4. Modeling

2.4.1. Titration modeling

A modified version (FITMOD) of the computer program FITEQL 2.0 (Westall, 1982) was used to construct SCMs describing proton interactions with bacteria. FITMOD permitted simultaneous modeling of systems with different solid-to-solution ratios and ionic strengths. The program employed the Donnan electrostatic model in which proton-active sites are assumed to be uniformly distributed through a volume, rather than concentrated into a single plane immediately at the bacteria–water interface (Ohshima and Kondo, 1991; Ohshima, 1995, 2002; Plette et al., 1995; van der Wal et al., 1997a; Wonders et al., 1997; Wasserman and Felmy, 1998; Martinez et al., 2002; Yee et al., 2004). The Donnan electrostatic model is applicable to biological cells because it accounts for the ion-penetrable layers of cross-linked ionizable functional groups covering bacterial surfaces. It also accounts for variation of controlling parameters such as pH and ionic strength by explicitly

describing the chemical reactions that occur between the solute and specific sites on the surface of interest.

Deprotonation reactions for surface functional groups within the Donnan volume were modeled by the following general chemical reaction and mass action law:

$$R-L_nH^x \Longleftrightarrow R-L_n^{x-1} + H^+ \tag{1}$$

$$K_n = \frac{[R-L_n^{x-1}]a_{H^+}}{[R-L_nH^x]}, \tag{2}$$

where R represents the bacterial cell wall to which the functional group L_nH is attached, x represents the charge of the protonated functional group, K_n represents the deprotonation stability constant, brackets represent the concentration of the enclosed surface sites (mol L^{-1}), and a_{H^+} represents the activity of protons. These formulations have been successfully employed to describe proton adsorption onto mesophilic bacteria (Fein et al., 1997; Daughney et al., 1998, 2001; Wightman et al., 2001; Yee and Fein, 2001; Borrok et al., 2004a,b; Borrok and Fein, 2005) and other biological surfaces (e.g. Xue et al., 1998; Daughney et al., 2004). These formulations are also analogous to those used to describe proton interactions with mineral surfaces (Stumm and Morgan, 1996; Langmuir, 1997).

The effect of the bacterial surface electric field on protonation reactions was accounted for using the following equation (Stumm and Morgan, 1996):

$$K_n^{int} = K_n \exp(-ZF\psi_D/RT). \tag{3}$$

Here, K_n^{int} is the intrinsic equilibrium constant referenced to zero surface charge and zero surface coverage. The variables Z, F, ψ_D, R, and T refer to the charge of the adsorbing ion, Faraday's constant, the electric potential at the location of adsorption (i.e. the Donnan potential), the gas constant, and the absolute temperature, respectively. For symmetrical electrolytes, the electric potential within the Donnan shell (ψ_D) was calculated from (Ohshima, 2002)

$$\psi_D = \frac{RT}{zF} \ln \left[\frac{Z\rho_D}{2zc} + \left\{ \left(\frac{Z\rho_D}{2zc} \right)^2 + 1 \right\}^{1/2} \right], \tag{4}$$

where z is the electrolyte valency, ρ_D is the charge density within the Donnan shell (C m^{-3}), and c is the electrolyte concentration (mol m^{-3}). The value of ρ_D was determined from the experimental proton titration data, the biomass concentration and the thickness of the Donnan shell, and was optimized during the modeling. In this study, we assumed the thickness of the Donnan shell to be equal to the thickness of the cell wall (Plette et al., 1995; van der Wal et al., 1997a; Wasserman and Felmy, 1998; Martinez et al., 2002; Yee et al., 2004).

In addition to the features described above, all models constructed for this investigation bore certain similarities. All stability constants were adjusted for ionic strength using the Davies equation (Langmuir, 1997), and all values tabulated in this paper were referenced to zero ionic strength, zero surface charge, and 25 °C. All models

included equilibria describing the dissociation of water, the acid, the base, and the electrolyte, with stability constants taken from the Critical Stability Constants Database (Smith and Martell, 1976). Model values for deprotonation constants and site concentrations were determined for several independent titrations, and the results were used to calculate uncertainties (2σ errors).

FITMOD was used to compare the fit of each model to the experimental data. FITMOD calculates the overall variance $V(Y)$ of the error (Y) in the chemical mass balance equations and therefore provides a quantitative estimate of the accuracy of the fit. For models involving mineral surfaces, values of $V(Y)$ between 1 and 20 indicate reasonable fits to the data (Westall, 1982).

2.4.2. Electrophoretic mobility modeling

We were unable to develop models for the electrophoretic mobility data alone because the relevant equations included several parameters that could not be determined from our experimental data. Instead, we used reasonable estimates of these parameters (based on information available in the literature), and made predictions for electrophoretic mobility based on the models developed to describe the titration data. We employed an iterative approach, based on the equations described below, to compare predicted electrophoretic mobility to the actual experimental data. The goal was to investigate whether or not the model developed to describe the titration data could also provide a reasonable estimation of the electrophoretic mobility data.

The electrophoretic mobility of a charged particle depends on the potential at the shear plane (zeta potential), not on the potential at the particle surface (Takamura and Chow, 1985; Ohshima and Kondo, 1991; Ohshima, 1995, 2002; Plette et al., 1995; Stumm and Morgan, 1996; van der Wal et al., 1997a,b; Yee et al., 2004). The zeta potential (ζ) is related to the potential at the surface (ψ_0) by (Takamura and Chow, 1985; Daughney, 2000)

$$\zeta = \frac{2RT}{F} \ln \frac{1 + \gamma_0 \exp(-\kappa x)}{1 - \gamma_0 \exp(-\kappa x)}, \tag{5}$$

where x represents the distance of the shear plane from the surface, κ is the reciprocal Debye screening length given by

$$\kappa^2 = \frac{2cz^2 F^2}{\varepsilon_r \varepsilon_0 RT}, \tag{6}$$

where ε_r is the relative permittivity of the electrolyte solution and ε_0 is the permittivity of a vacuum, and

$$\gamma_0 = \frac{\exp(F\psi_0/2RT) - 1}{\exp(F\psi_0/2RT) + 1}. \tag{7}$$

The surface potential was calculated from the Donnan potential as follows (Ohshima, 2002):

$$\psi_0 = \psi_D + \frac{2RTc}{Z\rho_D F} \left(1 - \left[\left\{\frac{Z\rho_D}{2zc}\right\}^2 + 1\right]^{1/2}\right). \tag{8}$$

Analyses are complicated by the unknown position of the plane of shear (Takamura and Chow, 1985; van der Wal et al., 1997a). To obtain the best fit to our experimental data, we chose the position of the shear plane to be 5 Å within the membrane. This value was varied over a reasonable range (see Takamura and Chow, 1985) during the modeling. Additionally, we assumed that the site spatial distribution was uniform throughout the cell wall, as proposed by other researchers (Plette et al., 1995; Wasserman and Felmy, 1998; Martinez et al., 2002; Yee et al., 2004), and that the cell wall thickness was a constant unaffected by electrolyte concentration.

Biological cells are analogous to 'soft' particles that are covered with an ion penetrable polyelectrolyte layer (the Donnan layer) (Ohshima and Kondo, 1991; Ohshima, 1995, 2002; Plette et al., 1995; van der Wal et al., 1997a; Wasserman and Felmy, 1998; Martinez et al., 2002; Daughney et al., 2004; Yee et al., 2004). Consequently, in this paper, the electrophoretic mobility μ was calculated from the zeta potential (ζ) using (van der Wal et al., 1997b)

$$\frac{\eta F}{\varepsilon_r \varepsilon_0 RT} \mu = \frac{F\zeta}{RT} + \frac{2\mathrm{Rel}}{1 + 2\mathrm{Rel}}$$
$$\times \left\{\frac{2}{z}\ln 2 - \frac{2}{z}\ln\left(1 + \exp\left(\frac{zF\zeta}{2RT}\right)\right)\right\}, \tag{9}$$

where η is the viscosity of the electrolyte solution and Rel is the surface conduction parameter. The surface conduction parameter is related to the mobile counter-charge density in the electrical double layer given by (van der Wal et al., 1997b,c)

$$\mathrm{Rel} = \frac{1}{\kappa a}\left[\left(1 + \frac{K^{\sigma,i}}{K^{\sigma,d}}\right) + 3\frac{m}{z^2}\right]\left[\exp\left(\frac{zF\zeta}{2RT}\right) - 1\right], \tag{10}$$

where a is the particle radius, $K^{\sigma,i}/K^{\sigma,d}$ is the conductivity ratio of countercharges beyond and behind the shear plane ($K^{\sigma,i}$ is the cell wall conductivity and $K^{\sigma,d}$ is the conductivity caused by the diffuse counterions), and m is the non-dimensional ionic drag coefficient. For Rel calculations, the effective particle radius was assumed to be 2 μm (approximately half the cell length), the conductivity ratio was assumed to be 75 based on the value for *Bacillus brevis* (van der Wal et al., 1997c), and m was assumed to be 0.16, as quoted for KNO_3 at 298 K (van der Wal et al., 1997b). These parameters were varied over a reasonable range during the modeling. The permittivity of the electrolyte solution within the Donnan membrane could not be determined from our experimental data, so was assumed equivalent to the permittivity of water in the bulk solution.

3. Results and discussion

3.1. Characteristics of the bacteria

Based on the growth curves (data not shown) the cells were in late stationary phase at the time of harvest. There was no evidence of sporulation. Note that cells were

intentionally harvested in late stationary phase to permit comparison with previous investigations involving mesophiles cultured to the same condition. Cells were rod-shaped with an average length and width of 3.89 ± 1.45 and 0.54 ± 0.18 μm, respectively (all standard deviations quoted here and throughout the paper are $\pm 2\sigma$, unless otherwise stated). Bacterial cells in this growth phase were determined to have an average cell wall thickness of 28.1 ± 7.4 nm based on multiple TEM thin sections. We acknowledge that cell wall volume might change with ionic strength, or that the ethanol dehydration procedure might influence cell wall thickness as measured by TEM. However, our cell dimensions are comparable to those reported for other bacterial species. Fein et al. (1997), Wightman et al. (2001), and Yee et al. (2004) report a cell dimension of 5×1 μm for *B. subtilis*. Wightman et al. (2001) also report a cell dimension of 2×1 μm for a thermophilic isolate and van der Wal et al. (1997a,b,c) report cell dimensions averaging 6×2 μm for a host of bacterial species. Our measured cell wall thickness agrees well with that reported for other bacterial cells: 25 nm (Beveridge, 1981 cited in Yee et al., 2004) and 35 to 75 nm (van der Wal et al., 1997a,b).

By approximating the cells as cylinders and by assuming a cell density of 1000 kg m^{-3}, we estimate a surface area of ~ 7.92 m^2 per wet g (propagation of 1σ errors yielded surface area values ranging from 6.78 to 9.52 m^2 g^{-1}). This estimate of surface area is lower than estimates for other bacteria, which range from 30 m^2 g^{-1} (Châtellier and Fortin, 2004) to 290 m^2 g^{-1} (Wightman et al., 2001).

Experimental data of cultures with this growth period indicate that the dry biomass present in a suspension is 0.5359 times its OD$_{600}$. All bacterial concentrations were derived from OD$_{600}$ using this relationship. The ratio of wet to dry mass of the bacteria was found to be 6.7 ± 0.1 to 1, in good agreement with literature values for other species: 9.9 ± 1.1 to 1 (Fein and Delea, 1999), 10.2 ± 0.8 to 1 (Daughney et al., 2001), and 5 to 1 (Borrok et al., 2004a; Borrok and Fein, 2005).

Based on confocal laser scanning microscopy investigations, the majority of the bacterial cells remain intact throughout the duration of the titrations, regardless of pH or electrolyte concentration. These results are in agreement with Borrok and Fein (2005), who used environmental scanning electron microscopy to confirm that cells of several mesophilic species remained visually intact after titrations. The lectin stain also revealed the presence of minimal extracellular polysaccharides. Note that we assume intact, non-viable cells will interact with protons identically to cells that are intact and viable, but metabolically inactive.

To investigate the possible release of exudates and metabolites from rinsed cell suspensions, we measured dissolved organic carbon (DOC) concentrations in filtrates after bacterial suspensions were equilibrated for different times at various pHs and ionic strengths (results not tabulated). The control experiments revealed ca. 10 ppm DOC in the filtrates even immediately after the final rinse (pH 6, ionic strength 0.001, 0.01, or 0.1 M). DOC concentrations after 2 h of equilibration at pH 6 were not significantly different from the controls, regardless of ionic strength ($p > 0.1$). In contrast, 2 h equilibration at pH 3 or pH 9 resulted in a significant change in DOC relative to the controls. DOC decreased by ca. 50% relative to the controls after 2 h equilibration at pH 3, perhaps due to DOC adsorption onto the cells or the experimental apparatus. Conversely, DOC increased by ca. 50% relative to the controls after 2 h equilibration at pH 9, perhaps due to desorption from the cells or to cell lysis. The pH effects were not significantly affected by ionic strength ($p > 0.2$). Fein et al. (1997), Daughney and Fein (1998), and Daughney et al. (1998) did not detect organic exudates following titration of *B. subtilis*, possibly because different methods were employed in the assessments (High Performance Liquid Chromatography and optical microscopy).

3.2. Acid–base titrations

The experimental titration data show that the bacteria provide substantial buffering capacity over a wide pH range (Fig. 1a). Note that for clarity: (1) only three of the five data sets are displayed, (2) only every second data point is plotted; and (3) a curve for the blank electrolyte is not shown (it displayed virtually no buffering in the pH range of our investigation). Excellent agreement between the first and second up-pH titration of a single aliquot of bacterial suspension indicates complete reversibility of proton adsorption within the timescale of these experiments (ca. 2 h). Several studies involving other bacteria have also reported that proton adsorption reactions are completely reversible over a comparable time scale (Daughney and Fein, 1998; Daughney et al., 1998; Wightman et al., 2001; Claessens et al., 2004), although titrations of longer duration may be irreversible (Claessens et al., 2004). Excellent agreement is also observed between duplicate titrations of different aliquots from a single parent suspension, indicating that experimental reproducibility is very good. The desorption of protons indicates that acidic sites on the bacterial surface are buffering the suspension against addition of the base. The data in Fig. 1a also show that the degree of buffering increases with bacterial concentration. Similar relationships between buffering capacity, pH, and biomass have been observed for acid–base titrations conducted on several mesophilic bacterial species (Fein et al., 1997, 2005; Daughney and Fein, 1998; Daughney et al., 1998, 2001; Yee and Fein, 2001; Borrok et al., 2004a; Borrok and Fein, 2005).

The five titration data sets collected at 0.01 M ionic strength were modeled independently using FITMOD (Fig. 1a, Table 1). A three site model is required to fit each data set, indicating that there are at least three types of proton-active functional groups on the bacterial surfaces. Two-site models do not fit the data as well, and four-site models do not offer improved fits. Note that the number of sites required to fit the data may be dependent on the
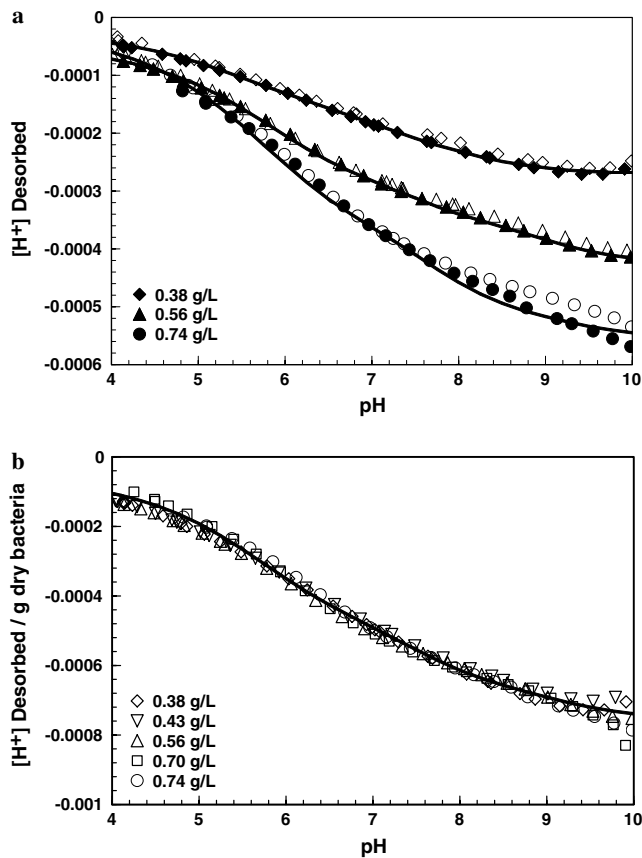
Fig. 1. Acid–base titration data (0.01 M) from independent cultures of *A. flavithermus*. Biomass concentrations are quoted in dry gram per litre. Solid lines represent best-fit model curves generated by FITMOD. (a) Data from three independent titrations, showing that the proton adsorption–desorption reactions are reversible and reproducible (for clarity, only every second data point is plotted; closed and open symbols represent the first and second up-pH titration, respectively). (b) Data from five independent cultures of *A. flavithermus* normalized to biomass (for clarity, only every second data point is plotted and only data from the first up-pH titration is shown).

pH range of the titration. Consequently, the models presented here are relevant to the range $4 < \text{pH} < 10$. Based on the magnitudes of the deprotonation constants and the fact that *A. flavithermus* is a Gram-positive bacterium, we speculate that the proton-active functional groups might correspond to carboxyl, phosphoryl, and amino sites. These functional groups are expected to be present because Gram-positive bacteria possess a thick peptidoglycan cell wall that contains polymers of sugars and cross-links of short peptides, in addition to teichoic and teichuronic acids (Beveridge and Murray, 1980; Beveridge et al., 1982; Beveridge, 1989; Plette et al., 1995; van der Wal et al., 1997a; Daughney et al., 1998; Chapelle, 2001; Wilson et al., 2001; Yee et al., 2004). Other researchers have reported similar number of sites with similar deprotonation constants for several mesophilic bacteria (e.g. Fein et al., 1997; Daughney et al., 1998; Châtellier and Fortin, 2004) and one other thermophile (Wightman et al., 2001). However, we acknowledge that spectroscopic data are required to clarify the identity of the titratable groups.

The models for the individual 0.01 M titrations yielded similar values for the deprotonation constants and concentrations for each distinct type of site, so we attempted to simultaneously model all five data sets with a single set of model parameters. Again, invoking a three-site model provides sufficient complexity to describe the data (Fig. 1b, Table 1). The titration data are expected to be comparable when normalised to biomass concentration. Because replicate titrations of a suspension from a single culture show excellent agreement (Fig. 1a), experimental error is small and the 2σ values presented in Table 1 represent the effect of inter-culture variability instead of experimental uncertainty. The single best-fitting model for all five titrations conducted at 0.01 M has an overall variance of 10.2, which is higher than the variance of any single model developed for an individual titration.

Table 1
Model parameters describing acid–base titrations of *A. flavithermus*

Trial[a]	g/L[b]	pK_1[c]	pK_2[c]	pK_3[c]	C_1[d]	C_2[d]	C_3[d]	$V(Y)$[e]
1	0.74	4.38	6.17	7.74	4.73	2.22	0.53	4.8
2	0.70	4.55	6.87	8.14	5.32	1.84	0.72	3.9
3	0.56	4.40	6.06	7.54	4.89	1.47	1.22	3.7
4	0.43	4.18	5.74	7.14	3.93	2.32	0.92	6.2
5	0.38	4.15	5.73	6.84	3.94	2.26	0.98	3.5
1–5 model	—	4.34 ± 0.33	6.04 ± 0.93	7.60 ± 1.02	4.57 ± 1.22	2.07 ± 0.72	0.88 ± 0.52	10.2
6	0.21	5.04	7.08	7.75	5.52	1.61	1.35	20.4
7	0.21	5.08	7.11	7.95	5.75	1.33	1.60	15.3
8	0.29	4.76	6.60	7.70	4.90	2.15	1.34	19.4
6–8 model[f]	—	4.94 ± 0.34	6.85 ± 0.57	7.85 ± 0.26	5.33 ± 0.87	1.79 ± 0.84	1.42 ± 0.29	15.5

[a] Trials 1–5 were individual titrations at 0.01 M that were modeled independently; Model 1–5 is the best fit with 2σ errors to all data points from trials 1–5 modeled simultaneously. Trials 6–8 were individual ionic strength titrations, each modeled independently, and model 6–8 is the best fit with 2σ errors to all data points from trials 6–8.
[b] Weight of dry bacteria per litre of electrolyte.
[c] pK values for the subscripted surface functional groups, corresponding to the condition of zero ionic strength and zero surface charge.
[d] Absolute concentrations of the subscripted surface functional groups in $\times 10^{-4}$ moles per gram of dry bacteria.
[e] Variance as calculated by FITMOD.
[f] Best fitting parameters for all titrations.

However, the model based on simultaneous fitting of all five 0.01 M titrations is more sophisticated than the models generated for the individual titrations because it accounts for differences in bacterial concentration (0.38–0.74 dry g L^{-1}) and inter-culture variability over the pH range investigated. Other researchers have proposed a single model to fit titrations of different biomass concentrations (Fein et al., 1997; Daughney and Fein, 1998; Daughney et al., 1998, 2001; Wightman et al., 2001; Borrok and Fein, 2005).

Titration of cells from a single culture in suspensions with equivalent biomass but different ionic strength display distinctly different buffering capacities (Fig. 2). Specifically, we observe that an increase in ionic strength results in more significant buffering capacity, as is commonly observed for mineral surfaces such as aluminas, kaolinites, and silicas (Abendroth, 1970; Fuerstenau, 1970; Bolland et al., 1980; James and Parks, 1982). Few previous studies have focused on the effect of ionic strength on acid–base titrations of bacteria, so it is unclear if our results match the behaviour generally observed for bacteria. For *B. subtilis* and *Bacillus licheniformis*, Daughney and Fein (1998) observed a decrease in total apparent site concentration with decreasing ionic strength (0.1–0.01 M) resulting in less buffering capacity observed at lower ionic strengths for a given pH value, in agreement with our data. Likewise, Martinez et al. (2002) observed a similar trend for *Escherichia coli*: the total site concentration at 0.01 M was slightly lower than at higher ionic strengths studied (up to 0.5 M). However, Martinez et al. (2002) also observed the opposite behaviour for *B. subtilis* titrated under the same range of ionic strengths. In contrast, no significant differences were observed in the acid–base titration curves of *Pseudomonas putida* and *Pseudomonas mendocina* as ionic strength varied from 0.01 to 0.5 M (Borrok and Fein, 2005) or for
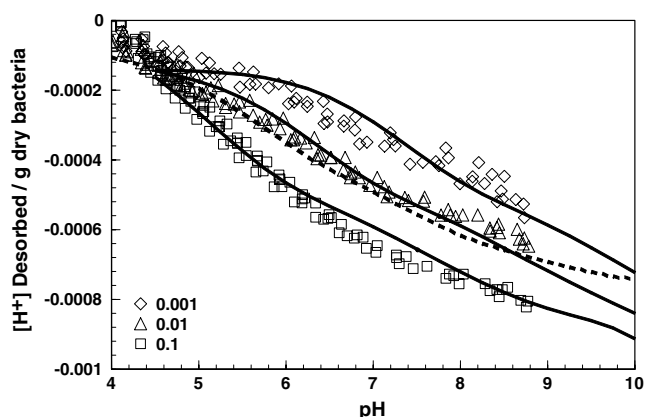

Fig. 2. Biomass-normalized acid–base titration data at three different ionic strengths (0.001, 0.01, and 0.1 M) for *A. flavithermus*. Data compiled from three suspensions with each suspension being a mixture of two independent cultures. Titrations at three different ionic strengths (0.001, 0.01, and 0.1 M) were conducted on each suspension. For clarity, five data points less than pH 4.5 have been omitted from each titration. Solid line represents model curve generated by FITMOD to fit all the data simultaneously, and is a three site model. Dashed line represents the model fit curve from Fig. 1b.

B. subtilis as ionic strength varied from 0.001 to 0.1 M (Yee et al., 2004) and 0.01 to 0.3 M (Fein et al., 2005).

We attempted to model all the ionic strength titrations with a single SCM. As with the independent titrations conducted at 0.01 M ionic strength, we began by modeling data from the three independent trials separately. Each trial consisted of data from six titrations, that is, duplicate titrations at ionic strengths 0.001, 0.01, and 0.1 M. Two σ errors are not reported for individual trials because duplicate titrations of the same suspension yield virtually identical results. These SCMs, based on the Donnan shell electrostatic model, were able to describe the ionic strength dependence of the titration data, using a single set of $\log K$ values and site concentrations for each trial (Table 1). Note that the choice of model parameters is not necessarily unique for all data sets. That is, several combinations of values for the deprotonation constants and site concentrations can yield a comparable fit to the titration data. The value of the deprotonation constant for site three was the hardest to constrain because the pK_a is close to the upper pH limit of our titration range (and possibly because cell lysis may occur when the pH is greater than ca. 9).

Finally, we attempted to develop a single SCM that could simultaneously match all of the data from all three ionic strength trials (Fig. 2). Note that the model curves in this figure are not developed separately for each ionic strength. Instead, the model curves were generated from a single set of model parameters. Note also that the model curves displayed in Fig. 2 are extended to pH 10 to allow for comparison with other datasets. The best fitting model had deprotonation constants (pK_a) of 4.94, 6.85, and 7.85 and site concentrations of 5.33×10^{-4}, 1.79×10^{-4}, and 1.42×10^{-4} mol per dry g for sites one, two, and three, respectively (Table 1). In general, the model provides an adequate fit to the data collected over the ionic strength range 0.001–0.1 M with an overall variance of 19.5. It also sufficiently fits the experimental data from the 0.01 M titrations with a variance of 32.1. Applying the previous best-fitting model generated from the 0.01 M titrations yielded a variance of 52.4 to the ionic strength titrations. Hence, the model generated to fit the ionic strength titrations is more robust in that it can completely describe acid–base behaviour as a function of pH and ionic strength within the limits considered in this investigation. Having identified a set of pK_a values and site concentrations that could provide a reasonable fit to all of the experimental titration data, we investigated whether or not these same parameters could also describe electrophoretic mobility measurements made on the bacterium. It is useful to make a semi-quantitative comparison to the electrophoretic mobility data to evaluate the robustness of certain assumptions we made to model the titration data (see below).

Although the Donnan model has been employed extensively to describe ion adsorption by biological colloids (Ohshima and Kondo, 1991; Ohshima, 1995, 2002; Plette et al., 1995; van der Wal et al., 1997a; Wonders et al., 1997; Wasserman and Felmy, 1998; Martinez et al.,

2002; Daughney et al., 2004; Yee et al., 2004), our results provide the first demonstration of the Donnan model's ability to describe the ionic strength dependence of proton adsorption by a thermophilic bacterium. The ability of the SCM to match data over a range of ionic strength provides clear support for the application of an electrostatic model, but does not imply that the Donnan shell model is superior to any other electrostatic models. It is beyond the scope of this study to compare different electrostatic models, although this topic has been addressed in the past. For example, Daughney and Fein (1998) attempted to account for the effects of ionic strength on proton adsorption using the Constant Capacitance and Stern models. These authors found that neither electrostatic model could match data from different ionic strengths with a single set of SCM parameters. Borrok and Fein (2005) found that bacterial surface electric field effects were negligible for proton adsorption onto *P. putida* and *P. mendocina*, and concluded that a non-electrostatic model was adequate to describe the data. Plette et al. (1995) successfully employed the Donnan model to account for the significant electrostatic effect of different ionic strengths (0.01–1 M) on the cell wall charge of *Rhodococcus erythropolis*. In that study, the cell wall charge became increasingly negative at higher ionic strengths, which is in agreement with our data. Martinez et al. (2002) also employed the Donnan model to describe the titrations of other mesophilic bacteria, *B. subtilis* and *E. coli*, as a function of ionic strength (0.01–0.5 M). In conclusion, based only on titration data collected over a narrow range of ionic strengths, it is difficult if not impossible to determine what type of electrostatic model is most appropriate for bacterial surfaces, or indeed if a non-electrostatic model is more suitable.

The possible effect of DOC on the titrations, and implications for model development, must be carefully considered. Recall that titrations were observed to be fully reversible (Fig. 1a). This indicates that: (1) no additional proton-reactive ligands are introduced to the system during the titrations, regardless of pH or ionic strength, and (2) changes in pH or ionic strength do not cause any irreversible changes to the binding characteristics of the proton-reactive ligands in the system. Thus it is possible that DOC, although present, is unreactive towards protons under our experimental conditions, such that all proton-reactive ligands in the system are in fact associated with the bacterial surfaces. Alternatively, the DOC might be proton reactive, in which case our model describes proton distribution in a system containing bacteria and fixed concentration of DOC, with the latter moving between being sorbed at low pH and desorbed at high pH (see above). This behaviour of DOC would be consistent with the behaviour of fulvic and humic acids in the presence of bacteria, as described by Fein et al. (1999), Wightman and Fein (2001), and Frost et al. (2003). Regardless of which scenario is correct, we have covered a broad range of experimental conditions in terms of pH and ionic

strength, and so the SCM developed to describe the data should be relevant to a range of natural conditions.

3.3. Electrophoretic mobility

The electrophoretic mobility data indicate that bacteria acquire a pH dependent charge and are dominantly electronegative in the pH range studied (Fig. 3a). The surface charge becomes increasingly negative with increasing pH, which has been reported for other biological surfaces (van der Wal et al., 1997b; Busscher et al., 2000; Daughney et al., 2004; Yee et al., 2004). Additionally, electrophoretic mobility decreases with increasing ionic strength. This relationship between the electrophoretic mobility and ionic strength is similar to that which has been observed by van der Wal et al. (1997b) and Yee et al. (2004). At higher ionic strengths, more counter ions are electrostatically adsorbed, reducing the electrical potential of the cell wall (Yee et al., 2004). The isoelectric point (IEP) of the bacteria was found to be ∼3.0 based on the intersection of regression lines through the experimental data. This IEP
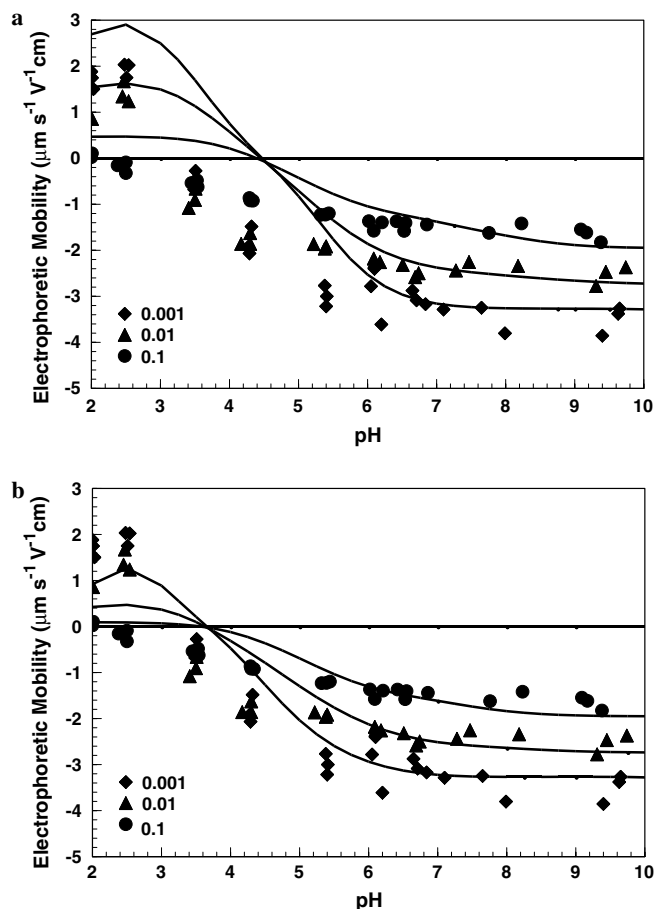

Fig. 3. Electrophoretic mobility data at three different ionic strengths (0.001, 0.01, and 0.1 M) for three independently grown cultures of *A. flavithermus*. (a) Solid lines represent predicted electrophoretic mobilities based on the SCM that best describes the titration data (Table 2). (b) Solid lines represent predictions of electrophoretic mobilities based on the SCM if the concentration of the third site is reduced by 80%.

is similar to that of other Gram-positive bacteria described in the literature: ~2.4 for *B. subtilis* (Yee et al., 2004); 3.6, 3.4, and 4.6 for a *Cornebacterium* species, *Rhodococcus opacus*, and *B. brevis*, respectively (van der Wal et al., 1997a,b); and ~4.5 for *R. erythropolis* (Plette et al., 1995).

Qualitatively, the data are in agreement with the best-fitting SCM based on the titration data. The negative charge confirms the presence of anionic functional groups (e.g., carboxyl, phosphoryl) within the cell wall which can acquire negative charge when deprotonated. The existence of cationic functional groups, such as amino sites, is implied by the positive electrophoretic mobilities at the most acidic pH values. Further, the model deprotonation constants of 4.94, 6.85, and 7.85 are consistent with the values expected for carboxyl, phosphoryl, and amino sites, respectively. These types of sites have also been implicated in proton interactions with other biological surfaces (Shumate and Strandberg, 1985; Plette et al., 1995; Fein et al., 1997; Daughney et al., 1998, 2004; Cox et al., 1999; Martinez et al., 2002). Thus we conclude that electrophoretic mobility data are very useful for constraining the types of reactions to be included in an SCM, even if the comparison is strictly qualitative.

We use the best-fitting SCM based on the ionic strength titration data in an attempt to match the electrophoretic mobility data, using equations given in Section 2.4.2. We stress that we are unable to make a fully quantitative comparison between the SCM and the experimental data, because calculation of electrophoretic mobility from charge density (ρ_D) requires several assumptions that we cannot explicitly test. These assumptions include the equivalence of protonation behaviour and surface charge development, the uniformity of distribution of titratable sites through the membrane, the constancy of membrane volume as a function of ionic strength, and the lack of residual metabolic activity that might allow the cells to pump protons through the membrane. In addition, calculation of electrophoretic mobility from charge density requires knowledge of several parameters that we did not explicitly measure. We begin by assuming that: (1) the shear plane is coincident with the surface ($x = 0$ in Eq. (5)) such that surface potential ψ_0 equals the zeta potential ζ; (2) the conductivity ratio $K^{\sigma,i}/K^{\sigma,d}$ is 100, within the range of Gram-positive and Gram-negative bacteria measured by van der Wal et al. (1997c); (3) the mobility of $NaNO_3$ is 0.16, equivalent to the value given for 0.01 M KNO_3 by van der Wal et al. (1997b,c); and (4) the effective cell radius is approximately half the cell length ($a = 2.0 \times 10^{-6}$ m). We vary each of these parameters over a reasonable range to evaluate the effect on predicted electrophoretic mobility (-1 nm $< x <$ $+1$ nm; $15 < K^{\sigma,i}/K^{\sigma,d} < 300$; $0 < m < 1$).

We find that the SCM based on the titration data is able, to some extent, to predict our experimental electrophoretic mobility data (Fig. 3a). Specific discrepancies between the prediction and actual data are: (1) that the predicted IEP is roughly 1.4 pH units too high and (2) the predicted electrophoretic mobilities at pH < IEP are too large. The

parameter values that provided the best fit to the electrophoretic mobility data were $x = -0.5$ nm, $K^{\sigma,i}/K^{\sigma,d} = 75$, $m = 0.16$, and $a = 2.0 \times 10^{-6}$ m. In general, the calculated electrophoretic mobility values are insensitive to m, but are sensitive to: (1) the exact position of the shear plane for 0.1 M ionic strength and (2) the conductivity ratio and the effective cell radius for 0.01 and 0.001 M ionic strength when absolute electrophoretic mobilities are greater than 1.5. In other words, each parameter affects only small sections of the predicted electrophoretic mobility curves, such that it is possible to identify a unique best-fitting set of values for x, $K^{\sigma,i}/K^{\sigma,d}$ and a.

It is instructive to consider how certain changes in the SCM based on the titration data would affect the predicted electrophoretic mobilities. We note that if the concentration of the third site is reduced by ~80%, the fit to the electrophoretic mobility data is improved (Fig. 3b). Specifically, the predicted IEP is closer to the observed value by almost an entire pH unit and that there is only a slight overestimation of electrophoretic mobilities at pH values below the IEP. This may indicate that some of the sites are not uniformly distributed through the Donnan volume as we have assumed. Alternatively, an improved prediction of electrophoretic mobility (comparable to Fig. 3b) is obtained if we assume that the cell walls include a fixed source of negative charge, as would be consistent with the presence of functional groups that are fully deprotonated within the pH range of our experiments (i.e. $pK_a < $ ca. 3). The existence of sites with low pK_a has been proposed for other bacterial species (Borrok et al., 2004a,b; Fein et al., 2005), but determination of the concentration of such sites from titration data alone is problematic because the acidic conditions required to protonate the sites also damage the cell walls (Borrok et al., 2004b). Instead, our results suggest that it may be possible to estimate the concentration of low-pK_a sites on the basis of electrophoretic mobility data. For example, for our data an improved fit to the electrophoretic mobility is obtained if the SCM based on the titration data (Table 1) is modified to include a fourth type of proton-active site that acquires negative charge upon deprotonation and has $pK_a < 3$ and concentration ca. 1.25×10^{-4} mol per g dry biomass. We stress again that for reasons outlined above we are unable to quantitatively modify the SCM based on the titration data to obtain improved fits to the electrophoretic mobility data, but we conclude that useful qualitative information can be obtained using the approach we have employed in this investigation.

3.4. Comparison to other biological surfaces

The SCM that best fits all of the titration data was used as the basis for comparison to other biological surfaces (Table 2). The model curve for *A. flavithermus* was compared to model curves for: (1) the Gram-positive thermophile TOR-39 (Wightman et al., 2001); (2) the Gram-positive mesophile *B. subtilis* (Daughney et al.,

Table 2
Average surface characteristics of *A. flavithermus* and some biological surfaces

Species	*A. flavithermus*	TOR-39	*B. subtilis*	*B. licheniformis*	*E. coli*	*P. mendocina*	Six natural consortia
Source	This paper	Wightman et al. (2001)	Daughney et al. (2001)	Daughney et al. (1998)	Yee and Fein (2001)	Borrok and Fein (2005)	Borrok et al. (2004a)
Model[a]	3 pK/Donnan	3 pK/Constant capacitance	3 pK/Constant capacitance	3 pK/Constant capacitance	1 pK/Constant capacitance	4 pK/Non-electrostatic	4 pK/Non-electrostatic
pK_1[b]	—	—	—	—	—	2.86 ± 0.38	3.12 ± 0.26
pK_2	4.94 ± 0.34	4.5 ± 0.2	4.80 ± 0.10	5.2 ± 0.6	4.87	4.66 ± 0.14	4.70 ± 0.22
pK_3	6.85 ± 0.57	5.8 ± 0.1	6.49 ± 0.30	7.5 ± 0.8	—	6.33 ± 0.14	6.57 ± 0.34
pK_4	7.85 ± 0.26	8.2 ± 0.1	8.52 ± 0.60	10.2 ± 1.0	—	9.04 ± 0.08	8.99 ± 0.42
C_1[c]	—	—	—	—	—	4.54 ± 1.47	3.33 ± 1.96
C_2	5.33 ± 0.87	4.0 ± 2.7[d]	6.92 ± 3.98	8.88 ± 7.60	22.4	5.55 ± 0.24	3.39 ± 2.65
C_3	1.79 ± 0.84	3.4 ± 1.3	4.44 ± 2.65	8.34 ± 9.20	—	3.02 ± 0.18	1.84 ± 1.71
C_4	1.42 ± 0.29	2.0 ± 1.3	6.29 ± 2.24	12.7 ± 13.6	—	2.57 ± 0.12	2.24 ± 2.19
C_T[e]	8.54 ± 2.00	9.38 ± 5.36	17.6 ± 8.9	29.9 ± 30.4	22.4	15.7 ± 2.0	10.8 ± 8.5
SA[f]	N/A	290	140	140	140	N/A	N/A
C[g]	N/A	8.0	8.0	3.0	8.0	N/A	N/A

[a] Models consider one, three, or four distinct types of surface functional groups and are termed 1 pK, 3 pK, and 4 pK, respectively; Surface electric field was accounted for using the Donnan or Constant capacitance model; Borrok et al. (2004a) and Borrok and Fein (2005) did not account for electrostatic effects.

[b] Negative logarithm of the stability constant describing deprotonation of the subscripted functional group, with 2σ errors, corresponding to the condition of zero ionic strength and zero surface charge; Yee and Fein (2001) did not report errors for all model variables.

[c] Absolute concentrations of the subscripted surface functional groups, with 2σ errors, in $\times 10^{-4}$ moles per gram of dry bacteria; Yee and Fein (2001) did not report all errors.

[d] Daughney et al. (1998), Wightman et al. (2001), and Yee and Fein (2001) reported site densities in moles per gram of wet bacteria and did not state wet to dry weight ratio. The wet to dry weight ratio for *B. licheniformis* and *E. coli* is 10 to 1 (C. Daughney, Institute of Geological and Nuclear Sciences, pers. comm., 2005; N. Yee, Rutgers University, pers. comm., 2005) and we assume that TOR-39 has a wet to dry weight ratio of 6.7 to 1.

[e] Total site density, with 2σ errors, in $\times 10^{-4}$ moles per gram of dry bacteria.

[f] Surface area of the species (m^2 g^{-1} wet bacteria).

[g] Capacitance of surface (F m^{-2}).

2001); (3) the Gram-positive mesophile *B. licheniformis* (Daughney et al., 1998); (4) the Gram-negative mesophile *E. coli* (Yee and Fein, 2001); (5) the Gram-negative mesophile *P. mendocina* (Borrok and Fein, 2005); and (6) the universal proton adsorption behaviour for six natural consortia from Borrok et al. (2004a). All model curves are based on titrations conducted at room temperature, except for TOR-39 which was titrated at 50 °C. Wightman et al. (2001) demonstrated that the acidity constants for *B. subtilis* change only slightly over the range 30–75 °C, so we assume that the deprotonation constants for TOR-39 at room temperature and at 50 °C are similar. The universal adsorption curve reported by Borrok et al. (2004a) is for six natural bacterial consortia grown at room temperature, with each consortium being unique, but being a mixture of three to six species. Note that acid–base titrations were not conducted beyond pH 10 in any of these investigations, except for *B. licheniformis* (Daughney et al., 1998). However, the model curves are plotted to pH 12 to allow comparison of the plateau in each curve that occurs above pH ca. 10, where all sites are assumed to be fully deprotonated. It is important to recognise that previously published models are based upon titrations that cover different pH ranges, and so the model curves should be compared with caution.

Comparison of the model curves indicates that the two thermophiles (*A. flavithermus* and TOR-39) have similar buffering capacity as a function of pH. *A. flavithermus* and TOR-39 were grown at 60 and 55 °C, respectively. The difference in buffering capacity is probably not due to the 5 °C difference in growth temperature, but a difference in the total concentration of proton-active functional groups per unit weight of biomass. *A. flavithermus* has a total proton-active site concentration of 8.54×10^{-4} mol g^{-1} dry within the range $4 < \text{pH} < 10$, which is close but not equivalent to the site density reported for TOR-39 (9.38×10^{-4} mol g^{-1} dry, $2.5 < \text{pH} < 9$). Wightman et al. (2001) reported concentrations in moles per gram dry bacteria, but did not give a wet to dry weight ratio. For the purpose of comparing model curves, we assumed both thermophiles possessed the same wet to dry weight ratio (6.7:1). However, it is known that the wet to dry weight ratio varies significantly between species (Borrok et al., 2004a) with reported values ranging from 3.1:1 (Borrok et al., 2004a) to 11:1 (Fein and Delea, 1999). If our estimate for the wet to dry weight of TOR-39 is too high or low, then the model curve for TOR-39 would show less or more buffering, respectively, than depicted in Fig. 4.

The two thermophiles display significantly lower buffering capacity than the pure cultures of mesophilic (Gram-positive and Gram-negative) bacteria that have been studied (Fig. 4). Both *A. flavithermus* and TOR-39 have significantly lower total site concentrations than the pure mesophilic bacterial species maintained in the laboratory. However, *A. flavithermus* and the natural consortia of mesophilic bacteria investigated by Borrok et al. (2004a)
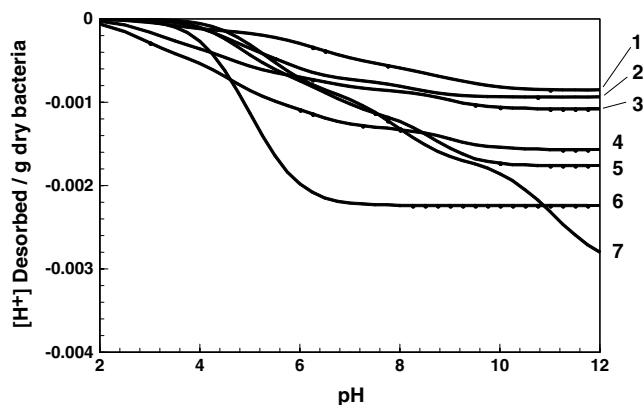
Fig. 4. FITMOD model output comparing the proton adsorption behaviour of *A. flavithermus* to other bacteria. Numbers to the right of the graph correspond to: (1) *A. flavithermus* (this study); (2) TOR-39 (Wightman et al., 2001); (3) an average adsorption curve for six natural consortia (Borrok et al., 2004a); (4) *P. mendocina* (Borrok and Fein, 2005); *B. subtilis* (Daughney et al., 2001); *E. coli* (Yee and Fein, 2001); and *B. licheniformis* (Daughney et al., 1998). The curves are calculated using the deprotonation constants and surface site concentrations summarized in Table 2, assuming 1 dry gram of biomass per litre of solution.

appear to have similar buffering capacities and similar total concentrations of proton-active functional groups per unit weight of biomass. To our knowledge, only two thermophiles have been investigated to date, so it is not yet clear whether thermophiles generally show different acid–base behaviour than mesophiles or if this is a phenomenon unique to the species chosen for study.

Aside from differences in total reactive site concentration, the model curves displayed in Fig. 4 also differ due to the number of sites considered and the values of stability constants describing their deprotonation. For instance, enhanced proton desorption is predicted below pH 4 for the natural bacterial consortia (Borrok et al., 2004a) and *P. mendocina* (Borrok and Fein, 2005) because these authors proposed a fourth site with pK_a ca. 3. Enhanced proton desorption is predicted above pH 10 for *B. licheniformis*. This results from deprotonation of the third site ($pK_a = 10.2$) which occurs approximately 1 to 2 pH units higher than in the other models. Notice also that the proton adsorption curve for *E. coli* plateaus at pH ca. 7, unlike the other models. This is because Yee and Fein (2001) proposed the deprotonation of only one site with pK_a ca. 5.

4. Conclusions

In this investigation, we characterized proton interactions with the thermophilic bacterium *A. flavithermus*. Our experiments indicate that a SCM is able to describe the proton adsorption–desorption behaviour of *A. flavithermus* over a wide range of pH and ionic strength. This SCM can also reasonably account for electrophoretic mobilities as a function of pH and ionic strength. This demonstrates that the model is robust and that the model parameters are well constrained. Our results also support

the use of the Donnan electrostatic shell model for bacterial surfaces.

It is not yet clear whether or not the SCM developed in this investigation will be applicable to natural environments. For example, the model may only be valid for cells grown to stationary phase on the selected growth medium (trypticase soy broth). Additionally, metabolically inactive cells might bind protons differently than metabolically active cells. On-going investigations in our laboratories are focused on determining if site densities on *A. flavithermus* (and other thermophiles) are affected by growth conditions (e.g., growth temperature, chemistry of the growth medium, presence of high metal concentrations) and if live cultures adsorb protons differently that non-active cultures.

Based on comparisons of these model parameters to those of another thermophile (TOR-39), *A. flavithermus* has comparable proton sorption characteristics. However, both thermophiles possess lower total site densities than pure cultures of mesophiles that have been studied to date. The differences in proton binding of thermophiles and mesophiles might be related to cell wall composition. Thermophiles have an unusual heat resistance (Brock, 1978) and, to survive high temperatures, have different cell wall configurations than mesophiles. It is well known that the fatty acid composition of cell membrane lipids depend on the growth temperature—thermophiles possess a increased proportion of fatty acids with higher melting points (and sometimes greater packing densities of phospholipids) than do lipids of mesophiles (Denich et al., 2003; Sundaram, 1986). Hence, thermophiles commonly have a greater abundance of long chain and saturated fatty acids within their membranes. The implications of these cell wall changes on surface charge and/or molecular groups titrated will be topics for future investigation.

It is also not yet clear whether the SCM developed in this investigation can be employed to predict interactions between *A. flavithermus* and metal ions or mineral surfaces. For example, if in fact the total site density of thermophilic bacteria is generally lower than mesophiles, this cannot be directly correlated to a reduction in metal biosorption capacity because the affinity of the metal for the binding site must also be taken into consideration. Indeed, to our knowledge, no previous investigations have reported a SCM describing metal adsorption by a thermophilic bacterium. Thus on-going investigations in our laboratories aim to determine whether *A. flavithermus* (and other thermophiles) sequester dissolved metals less or more effectively than mesophilic bacteria, and if metal adsorption is correlated to proton adsorption.

References

Abendroth, R.P., 1970. Behaviour of a pyrogenic silica in simple electrolytes. *J. Colloid Interface Sci.* **34**, 591–596.

Altschul, S.F., Gish, W., Miller, W., Myers, E.W., Lipman, D.J., 1990. Basic local alignment search tool. *J. Mol. Biol.* **215**, 403–410.

Banerjee, U.C., Chisti, Y., Moo-Young, M., 1993. Spectrophotometric determination of mycellial biomass. *Biotech. Tech.* **7**, 313–316.

Beveridge, T.J., Murray, R.G.E., 1980. Sites of metal deposition on the cell wall of *Bacillus subtilis*. *J. Bacteriol.* **141**, 876–887.

Beveridge, T.J., Forsberg, C.W., Doyle, R.J., 1982. Major sites of metal binding in *Bacillus licheniformis* walls. *J. Bacteriol.* **150**, 1438–1448.

Beveridge, T.J., 1989. Role of cellular design in bacterial metal accumulation and mineralization. *Annu. Rev. Microbiol.* **43**, 147–171.

Bolland, M.D.A., Posner, A.M., Quirk, J.P., 1980. pH-independent and pH-dependent surface charges on kaolinite. *Clays Clay Miner.* **28**, 412–418.

Borrok, D., Fein, J.B., Kulpa, C.F., 2004a. Proton and Cd adsorption onto natural bacteria consortia: testing universal adsorption behaviour. *Geochim. Cosmochim. Acta* **68**, 3231–3238.

Borrok, D., Fein, J.B., Tischler, M., O'Loughlin, E., Meyer, H., Liss, M., Kemner, K.M., 2004b. The effect of acidic solutions and growth conditions on the adsorptive properties of bacterial surfaces. *Chem. Geol.* **209**, 107–119.

Borrok, D.M., Fein, J.B., 2005. The impact of ionic strength on the adsorption of protons, Pb, Cd, and Sr onto the surfaces of Gram-negative bacteria: testing non-electrostatic, diffuse, and triple-layer models. *J. Colloid Interface Sci.* **286**, 110–126.

Brock, T.D., 1978. In: Starr, M.P. (Ed.), *Thermophilic Microorganisms and Life at High Temperatures*. Springer-Verlag, New York, NY.

Brock, T.D., 1986. Introduction: An overview of the thermophiles. In: Brock, T.D. (Ed.), *Thermophiles: General, Molecular, and Applied Microbiology*. John Wiley & Sons, pp. 1–16.

Busscher, H.J., Bos, R., van der Mai, H.C., Handley, P.S., 2000. Physiochemistry of microbial adhesion from an overall approach to the limits. In: Baszkin, A., Norde, W. (Eds.), *Physical Chemistry of Biological Interfaces*. Marcel Dekker, New York, NY, pp. 431–458.

Chapelle, F.H., 2001. *Ground-water Microbiology and Geochemistry*. John Wiley & Sons Inc., New York.

Châtellier, X., Fortin, D., 2004. Adsorption of ferrous ions onto *Bacillus subtilis* cells. *Chem. Geol.* **212**, 209–228.

Claessens, J., Behrends, T., van Cappellen, P., 2004. What do acid–base titrations of live bacteria tell us? A preliminary assessment. *Aquat. Sci.* **66**, 19–26.

Cox, J.S., Smith, D.S., Warren, L.A., Ferris, F.G., 1999. Characterizing heterogeneous bacterial surface functional groups using discrete affinity spectra for proton binding. *Environ. Sci. Technol.* **33**, 4514–4521.

Daughney, C.J., Fein, J.B., 1998. The effect of ionic strength on the adsorption of H^+, Cd^{2+}, Pb^{2+}, and Cu^{2+} by *Bacillus subtilis* and *Bacillus licheniformis*: A surface complexation model. *J. Colloid Interface Sci.* **198**, 53–77.

Daughney, C.J., Fein, J.B., Yee, N., 1998. A comparison of the thermodynamics of metal adsorption onto two common bacteria. *Chem. Geol.* **114**, 161–176.

Daughney, C.J., 2000. Sorption of crude oil from a non-aqueous phase onto silica: the influence of a aqueous pH and wetting sequence. *Org. Geochem.* **31**, 147–158.

Daughney, C.J., Fowle, D.A., Fortin, D., 2001. The effect of growth phase on proton and metal adsorption by *Bacillus subtilis*. *Geochim. Cosmochim. Acta* **65**, 1025–1035.

Daughney, C.J., Châtellier, X., Chan, A., Kenward, P., Fortin, D., Suttle, C.A., Fowle, D.A., 2004. Adsorption and precipitation of iron from seawater on a marine bacteriophage (PWH3A-P1). *Mar. Chem.* **91**, 101–115.

Denich, T.J., Beaudette, L.A., Lee, H., Trevors, J.T., 2003. Effect of selected environmental and physico-chemical factors on bacterial cytoplasmic membranes. *J. Microbiol. Methods* **52**, 149–182.

Fein, J.B., Daughney, C.J., Yee, N., Davis, T.A., 1997. A chemical equilibrium model for metal adsorption onto bacterial surfaces. *Geochim. Cosmochim. Acta* **61**, 3319–3328.

Fein, J.B., Delea, D., 1999. Experimental study of the effect of EDTA on Cd adsorption by *Bacillus subtilis*: a test of the chemical equilibrium approach. *Chem. Geol.* **161**, 375–383.

Fein, J.B., Boily, J.-F., Guclu, K., Kaulbach, E., 1999. Experimental study of humic acid adsorption onto bacteria and Al-oxide mineral surfaces. *Chem. Geol.* **162**, 33–45.

Fein, J.B., Boily, J., Yee, N., Gorman-Lewis, D., Turner, B., 2005. Potentiometric titrations of *Bacillus subtilis* cells to low pH and a comparison of modeling approaches. *Geochim. Cosmochim. Acta* **69**, 1123–1132.

Frost, P.C., Maurice, P.A., Fein, J.B., 2003. The effect of cadmium on fulvic acid adsorption to *Bacillus subtilis*. *Chem. Geol.* **200**, 217–224.

Fuerstenau, D.W., 1970. Interfacial processes in mineral/water systems. *Pure Appl. Chem.*, 135–164.

Haas, J.R., 2004. Effects of cultivation conditions on acid–base titration properties of *Shewanella putrefaciens*. *Chem. Geol.* **209**, 67–81.

James, R.O., Parks, G.A., 1982. Characterization of aqueous colloids by their electrical double layer and intrinsic surface chemical properties. In: Matijević, E. (Ed.), *Surface and Colloid Science*, vol. 12. Plenum Press, New York, pp. 119–216.

Langmuir, D., 1997. *Aqueous Environmental Geochemistry*. Prentice Hall, Upper Saddle River, NJ.

Madigan, M.T., 2000. Bacterial habitats in extreme environments. In: Seckbach, J. (Ed.), *Journey to Diverse Microbial Worlds*. Kluwer Academic Publishers, The Netherlands, pp. 63–74.

Martinez, R.E., Smith, D.S., Kulcycki, E., Ferris, F.G., 2002. Determination of intrinsic bacterial surface acidity constants using a Donnan shell model and a continuous pK_a distribution method. *J. Colloid Interface Sci.* **253**, 130–139.

Mountain, B.W., Benning, L.G., Boerema, J.A., 2003. Experimental studies on New Zealand hot spring sinters: rates of growth and textural development. *Can. J. Earth Sci.* **40**, 1643–1667.

Ohshima, H., Kondo, T., 1991. On the electrophoretic mobility of biological cells. *Biophys. Chem.* **39**, 191–198.

Ohshima, H., 1995. Electrophoretic mobility of soft particles. *Colloid Surf. A: Physiochem. Eng. Asp.* **103**, 249–255.

Ohshima, H., 2002. Electrokinetic behaviour of particles: theory. In: Hubbard, A.T., Somasundran, P. (Eds.), *Encyclopedia of Surface and Colloid Science*. Marcel Dekker, New York, NY, pp. 1834–1852.

Plette, A.C.C., van Riemsdijk, W.H., Benedetti, M.F., van der Wal, A., 1995. pH dependent charging behaviour of isolated cell walls of a Gram-positive soil bacterium. *J. Colloid Interface Sci.* **173**, 354–363.

Sampson, M.I., Phillips, C.V., 2001. Influence of base metals on the oxidising ability of acidophilic bacteria during the oxidation of ferrous sulfate and mineral sulfide concentrates, using mesophiles and moderate thermophiles. *Miner. Eng.* **14**, 317–340.

Smith, R.M., Martell, A.E., 1976. *Critical Stability Constants. IV: Inorganic Complexes*. Plenum Press, New York, NY.

Shumate, II.S.E., Strandberg, G.W., 1985. Accumulation of metals by microbial cells. In: Moo-Young, M. (Ed.), *Comprehensive Biotechnology: The Principles, Applications and Regulations of Biotechnology in*

Industry, Agriculture and Medicine. Elsevier, Amsterdam, pp. 235–247.

Stumm, W., Morgan, J.J., 1996. *Aquatic Chemistry, Chemical Equilibria and Rates on Natural Waters*, third ed. Wiley, New York.

Sundaram, T.K., 1986. Physiology and growth of thermophilic bacteria. In: Brock, T.D. (Ed.), *Thermophiles: General, Molecular, and Applied Microbiology*. John Wiley & Sons Inc., New York, pp. 1–16.

Takamura, K., Chow, R.S., 1985. The electric properties of the bitumen/water interface. Part II: application of the ionizable surface-group model. *Colloid Surf.* **15**, 35–48.

van der Wal, A., Norde, W., Zehnder, A.J.B., Lyklema, J., 1997a. Determination of the total charge in cell walls of Gram-positive bacteria. *Colloid Surf. B: Biointerfaces* **9**, 81–100.

van der Wal, A., Minor, M., Norde, W., Zehnder, A.J.B., Lyklema, J., 1997b. Electrokinetic potential of bacterial cells. *Langmuir* **13**, 165–171.

van der Wal, A., Minor, M., Norde, W., Zehnder, A.J.B., Lyklema, J., 1997c. Conductivity and dielectric dispersion of Gram-positive bacterial cells. *J. Colloid Interface Sci.* **186**, 71–79.

Wasserman, E., Felmy, A.R., 1998. Computation of the electrical double layer properties of semipermeable membranes in multicomponent electrolytes. *Appl. Environ. Microbiol.* **64**, 2295–2300.

Westall, J.C., 1982. FITEQL: A computer program for the determination of chemical equilibrium constants from experimental data: Version 1.2, Report 82-01, Department of Chemistry, Oregon State University.

Wilson, W.W., Wade, M.M., Holman, S.C., Champlin, F.R., 2001. Status of methods for assessing bacterial cell surface charge properties based on zeta potential measurements. *J. Microbiol. Methods* **43**, 153–164.

Wightman, P.G., Fein, J.B., 2001. Ternary interactions in a humic acid–Cd–bacteria system. *Chem. Geol.* **180**, 55–65.

Wightman, P.G., Fein, J.B., Wesolowski, D.J., Phelps, T.J., Bénézeth, P., Palmer, D., 2001. Measurement of bacterial surface protonation constants for two species at elevated temperatures. *Geochim. Cosmochim. Acta* **65**, 3657–3669.

Wonders, H.A.M., van Leeuwen, H.P., Lyklema, J., 1997. Metal- and proton-binding properties of a core-shell latex: interpretation in terms of colloid surface models. *Colloid Surf. A: Physiochem. Eng. Asp.* **120**, 221–233.

Xue, H.-B., Stumm, W., Sigg, L., 1998. The binding of heavy metals to algal surfaces. *Water Res.* **22**, 917–926.

Yee, N., Fein, J.B., 2001. Cd adsorption onto bacterial surfaces: A universal adsorption edge? *Geochim. Cosmochim. Acta* **65**, 2037–2042.

Yee, N., Fowle, D.A., Ferris, F.G., 2004. A donnan potential model for metal sorption onto *Bacillus subtilis*. *Geochim. Cosmochim. Acta* **68**, 3657–3664.